Biochemical and Biophysical Research Communications 463 (2015) 137–142

Contents lists available at ScienceDirect

Biochemical and Biophysical Research Communications

journal homepage: www.elsevier.com/locate/ybbrc

Enhancement of human mesenchymal stem cell infiltration into the electrospun poly(lactic-co-glycolic acid) scaffold by fluid shear stress

Min Sung Kim [a, b], Mi Hee Lee [a], Byeong-Ju Kwon [a, b], Min-Ah Koo [a, b], Gyeung Mi Seon [a, b], Jong-Chul Park [a, b, *]

[a] Cellbiocontrol Laboratory, Department of Medical Engineering, Yonsei University College of Medicine, Seoul 120-752, Republic of Korea
[b] Brain Korea 21 PLUS Project for Medical Science, Yonsei University College of Medicine, 134 Shinchon-dong, Seodaemun-gu, Seoul 120-752, Republic of Korea

ARTICLE INFO

Article history:
Received 4 May 2015
Available online 20 May 2015

Keywords:
Cell infiltration
Fluid shear stress
Human mesenchymal stem cell
PLGA scaffold
Mechanotaxis

ABSTRACT

The infiltration of the cells into the scaffolds is important phenomenon to give them good biocompatibility and even biodegradability. Fluid shear stress is one of the candidates for the infiltration of cells into scaffolds. Here we investigated the directional migration of human mesenchymal stem cells and infiltration into PLGA scaffold by fluid shear stress. The human mesenchymal stem cells showed directional migrations following the direction of the flow (8, 16 dyne/cm^2). In the scaffold models, the fluid shear stress (8 dyne/cm^2) enhanced the infiltration of cells but did not influence on the infiltration of Poly(lactic-co-glycolic acid) particles.

1. Introduction

A scaffold is one of the key components in the tissue engineering paradigm in which it can function as a template to allow new tissue growth and also provide temporary structural support while serving as a delivery vehicle for cells and/or bioactive molecules [1,2]. An ideal scaffold for tissue regeneration should possess mechanical properties similar to the tissues being replaced, good biocompatibility with surrounding tissue, large porosity and pore size for good infiltration of cells, high pore interconnectivity for tissue ingrowth, and biodegradability such that it is gradually replaced by growing tissues [3]. For a scaffold that requires minimal cellular infiltration (e.g., a vascular graft) and proliferation limited to the surface may be acceptable or even desirable. A large number of studies have been devoted to characterize the in vitro new tissue regeneration capability of hMSCs cultured within biodegradable porous scaffolds. The results of these studies evidenced that parameters such as surface topography and chemistry as well as hMSC seeding density and 3D spatial distribution/organization strongly influence cell–material interaction and extracellular matrix deposition [4–9]. Nevertheless, cell cultivation in 3D porous scaffolds is often impaired by the difficulty of achieving a homogeneous cell seeding and by the diffusion constraints within the cell–scaffold constructs [6,9–11].

Fluid shear stress enhances cell migration in the direction of flow and is called "mechanotaxis" [8]. Studies have shown that shear stress can regulate MSC proliferation and differentiation into osteoblasts, ECs, or cardiomyocytes [9–11], suggesting that MSCs are also sensitive to mechanical stress produced by fluid flow.

Human bone marrow-derived mesenchymal stem cells (hMSCs) are ideal candidates for tissue engineering research because they are multipotent, uncommitted cells with the ability to become specialized cells and which can be relatively easily isolated [12]. They contribute to the development, regeneration and maintenance of various mesenchymal tissues including cartilage, bone, muscle and adipose [4,5,13–16]. In this study, we investigated the effect of fluid shear stress on the migration of hMSCs and figure out the enhancement of hMSCs infiltration into PLGA scaffold by fluid shear stress.

2. Materials and methods

2.1. Cell culture

Human bone marrow-derived mesenchymal stem cell (hMSCs, Lonza, Basel, Switzerland) were cultured in Mesenchymal Stem Cell

Abbreviations: hMSC, human mesenchymal stem cell; PLGA, poly(lactic-co-glycolic acid).

* Corresponding author. Cellbiocontrol Laboratory, Department of Medical Engineering, Yonsei University College of Medicine, 134 Shinchon-dong, Seodaemun-gu, Seoul 120-752, Republic of Korea. Fax: +82 2 363 9923.
E-mail address: Parkjc@yuhs.ac (J.-C. Park).

http://dx.doi.org/10.1016/j.bbrc.2015.05.048
0006-291X/

Growth Medium (MSCGM, Lonza). Cells were incubated at 37 °C in a 5% CO_2 atmosphere. hMSCs between passages 5 and 9 were used in all experiments.

2.2. Applying the fluid shear stress to hMSCs

We used the parallel plate chamber system to apply shear stress to hMSCs [17]. The parallel plate chamber system was made of incubator system installed with the microscope to observe live cells and the flow chamber to apply shear stress to the cells. The incubator was regulated by temperature and gas composition controlling program (CCP ver. 3.8) under appropriate environment for the cells (CO_2 5%, 37 °C). The flow chamber consisted of the main body, bottom plate and silicon gasket (Fig. 1A). The main body had the inlet and outlet for tubing (inner diameter, 2 mm) to apply the fluid shear stress to the cells. The hMSCs were seeded on the coverslip before mounted on the bottom plate. The main body and the silicon gasket (200 μm in height, 2 mm in width) were combined with the coverslip and bottom plate together. The medium was flowed through the inlet and outlet tube.

2.3. Analysis of cell migration by fluid shear stress

The parallel plate chamber was placed on the microscope stage. The cell images were recorded every 5 min using a charge-coupled device (CCD) camera (Electric Biomedical Co. Ltd., Osaka, Japan) attached to an inverted microscope (Olympus Optical Co. Ktd., Tokyo, Japan). The images were stored to the computer by using the Tomoro image capture program; images were saved as JPEG files. Captured images were imported into ImageJ (ImageJ 1.37v by W. Rusband, National Institutes of Health, Bethesda, MD, USA). Image analysis was carried out by the manual tracking and chemotaxis tool plug-in (v. 1.01, distributed by ibidi GmbH, Munchen, Germany). The XY coordinates of each cell were obtained by using the manual tracking program. The data were imported into the chemotaxis plug-in. The cell migration speed was computed automatically and the cell migration pathway was plotted by the chemotaxis tool. The directedness of migration was assessed as cosine θ, where θ is the angle between the flow shear stress vector and a straight line connecting start and end positions of a cell (Fig. 1B). A cell moving directly to the down (direction of the flow) would have a directedness of 1; a cell moving directly to the up (opposite direction of

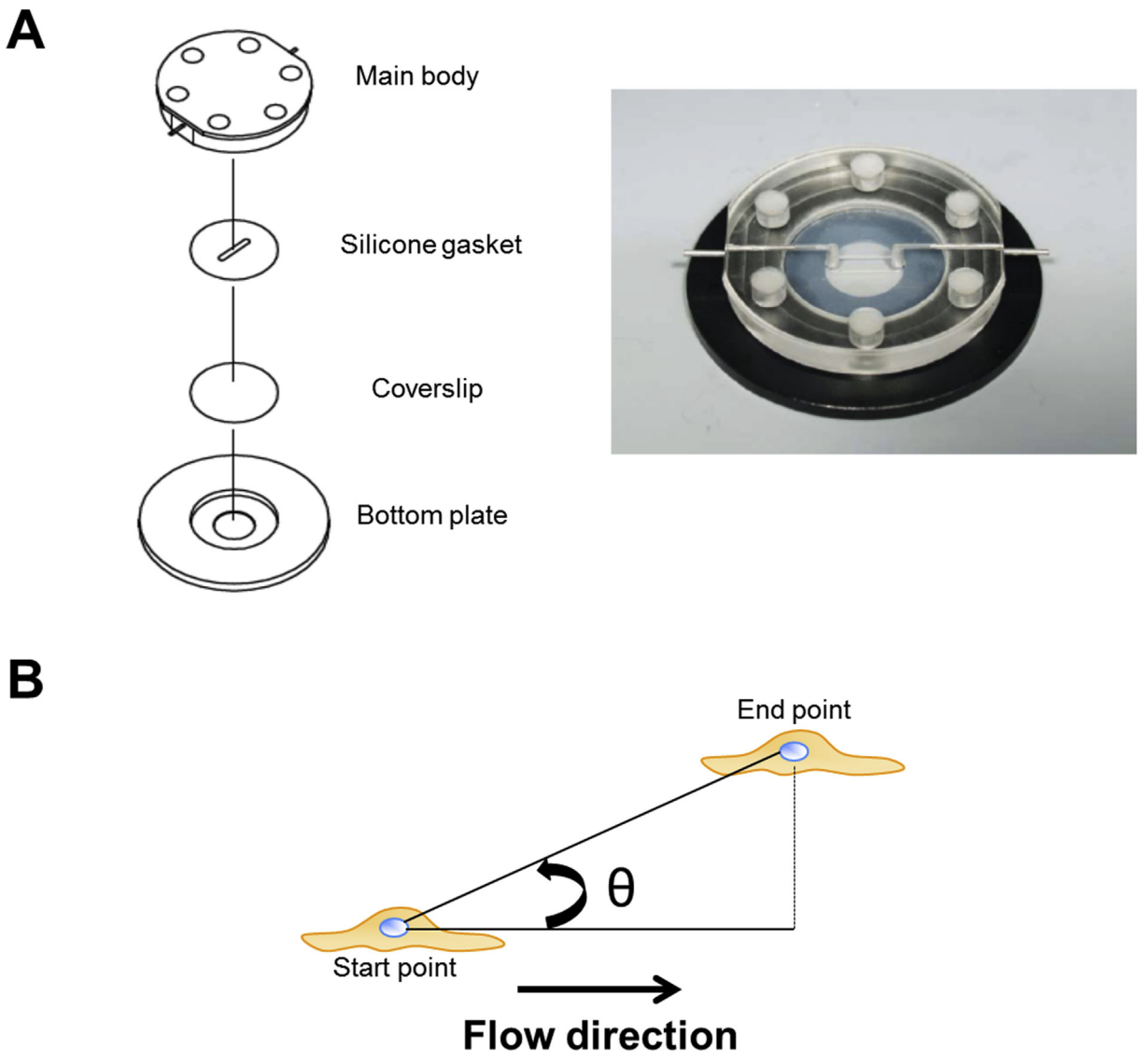

Fig. 1. The schematic of mechanotaxis chamber and directedness. (A) The parallel plate chamber system. (B) Schematic of the directedness.

the flow) would have a directedness of −1. The value close to 0 represents the random cell movement. Therefore, an objective quantification of how directionally cells have moved was given by the average directedness of a population of cells.

2.4. Electrospun PLGA scaffold

PLGA polymer (lactide/glycolide = 75:25) was purchased from Lakeshore Biomaterials (Birmingham, USA). PLGA was dissolved in a 1:4 mixture of dimethylforma-mide (DMF, Duksan Pure Chemicals co., Ltd., Ansan, Republic of Korea) and tetrahydrofuran (THF, Duksan Pure Chemicals co., Ltd., Ansan, Republic of Korea) at a concentration of 20% (w/v), and the mixture solvent was highly volatile. The polymer solution was then loaded into a syringe with 21 gauge metal needle tip. The needle tip was connected to 20 kV of a high-voltage source and a metal drum collector was served as the ground for the electrical charges. The distance between the needle tip and the drum collector was 10 cm, and the polymer solution was ejected at 2 mL/h. For the deposition of the ice crystals on the collector surface, the drum was loaded with dry ice which gives extremely low temperatures (−78.5 °C) to the drum surface. The environmental humidity was maintained at 50% approximately using a humidifier. After fabrication, the scaffolds containing ice crystals were lyophilized to maintain porous structure. The diameter of fibers was measured using the image J software program on basis of the scale bar.

2.5. PLGA particle containing green fluorescence fabrication

PLGA nanoparticles were prepared by an improved double-emulsion (water-in-oil-in-water) solvent extraction technique [18]. The 600 mg of PLGA (lactide/glycolide = 50:50) and 10 μl of Alexa (488)-conjugated phalloidin (Invitrogen, Carlsbad, CA) were dissolved in the dichloromethane (DCM, Duksan Pure Chemicals co., Ltd., Ansan, Republic of Korea). The mixed solution was vortexing for emulsion on a vortex mixer for 10 min. The emulsified solution was added gently with stirring into 50 ml of water containing 100 mg of poly(vinyl alcohol) (PVA, sigma-aldrich, Sigma−Aldrich, St Louis, USA) to form the water-oil-water emulsion. The re-emulsified solution was poured to 50 ml of water containing 1 ml of aqueous isopropanol solution (Duksan Pure Chemicals co., Ltd., Ansan, Republic of Korea) then stirred for 12 h to harden the PLGA particles. After hardening, the emulsion is then subjected to solvent removal by extraction process. The emulsion was centrifused (1200 rpm, 5 min) and the supernatant was removed by suction. The solid microspheres so obtained are then washed and collected by sieving using two micro-sieves (36 μm, 50 μm). These are then dried under freeze-drier for lyophilizing to give the final microsphere product and stored at 4 °C.

2.6. Scanning electron microscope

The surface and the cross-sectional morphology of electrospun PLGA scaffold and distribution of PLGA particles were observed with scanning electron microscope (SEM, S-4700, Hitachi, Tokyo, Japan). The porous scaffolds and PLGA particles were coated with PT by sputtering for 3 min before SEM observation.

2.7. Fluid shear stress on hMSC seeded PLGA scaffold

We used the peristaltic pump to provide the fluid shear stress to the hMSCs seeded PLGA scaffold. The chamber was tapered to

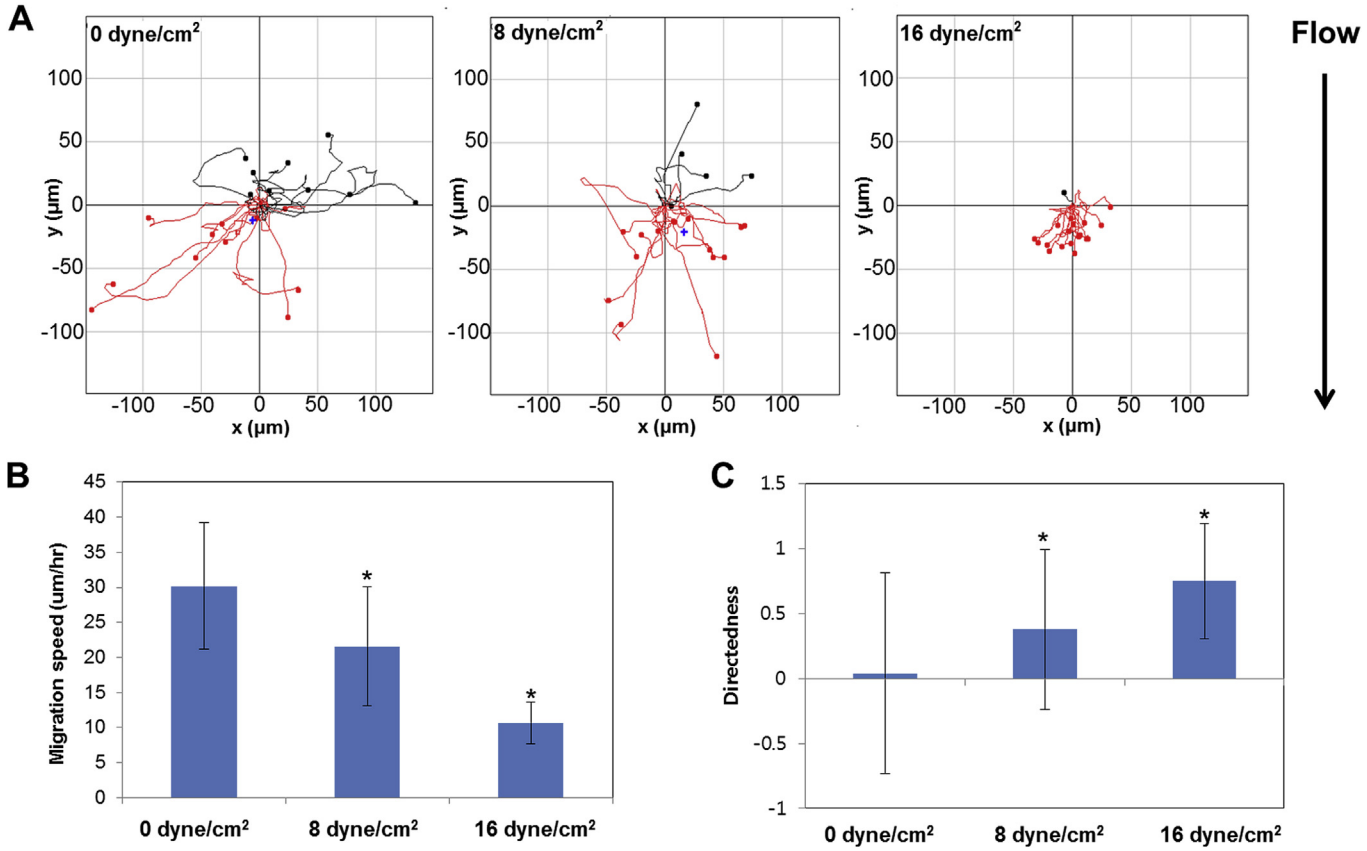

Fig. 2. The migration assay of hMSCs under flow condition (0, 8, 16 dyne/cm^2) for 4 h (A) 80 cells of each condition were tracked. (B) migration speed was measured, and (C) directedness was determined for hMSC under flow shear stress conditions for 4 h (0, 8, 16 dyne/cm^2). *$p < 0.05$ compared to controls grown with no flow shear stress (0 dyne/cm^2).

ensure flow from the outer edges of the scaffold as well as the center to the exit port of the chamber. The screw caps were fitted with silicon O-rings for a tight seal and prevention of leakage. The peristaltic pump pulled the medium from the reservoir and provided it to the chamber including hMSC seeded PLGA scaffold via 6 mm inner diameter silicon tubing. The culture medium was maintained at 37 °C and equilibrated with 5% CO_2 throughout the experiment. The equipment was sterilized by steam autoclave (tubing, chamber). The apparatus was assembled under sterile conditions in a laminar flow biosafety cleanbench.

2.8. Observation of the cells and PLGA particles in the scaffold

The cells were seeded on the PLGA scaffold (1×10^4 cells/scaffold, diameter of scaffold = 15 mm) and incubated in 5% CO_2 and 37 °C for 4 h 8 dyne/cm^2 of flow stress was applied to the cell seeded PLGA scaffold. After 12 h applying the flow shear stress, the scaffolds were washed 3 times with PBS and the cells were fixed with pre-cooled (−20 °C) 70% ethanol for 15 min. The PLGA scaffold was cryosectioned, then the cells were stained with propidium iodide (Sigma, Steinheim, Germany). The infiltration of cells and PLGA particles into the scaffold were observed by a confocal microscope (LSM 700, Carl Zeiss Micro Imaging Inc., Thornwood, NY, USA).

2.9. Statistical analysis

Data are reported as means ± standard error of the mean (SEM). The letter n denotes the number of tests, except in the migration assay where n denotes the number of cells. Means were compared using one-way analyses of variance (ANOVA). Two-tailed Student's

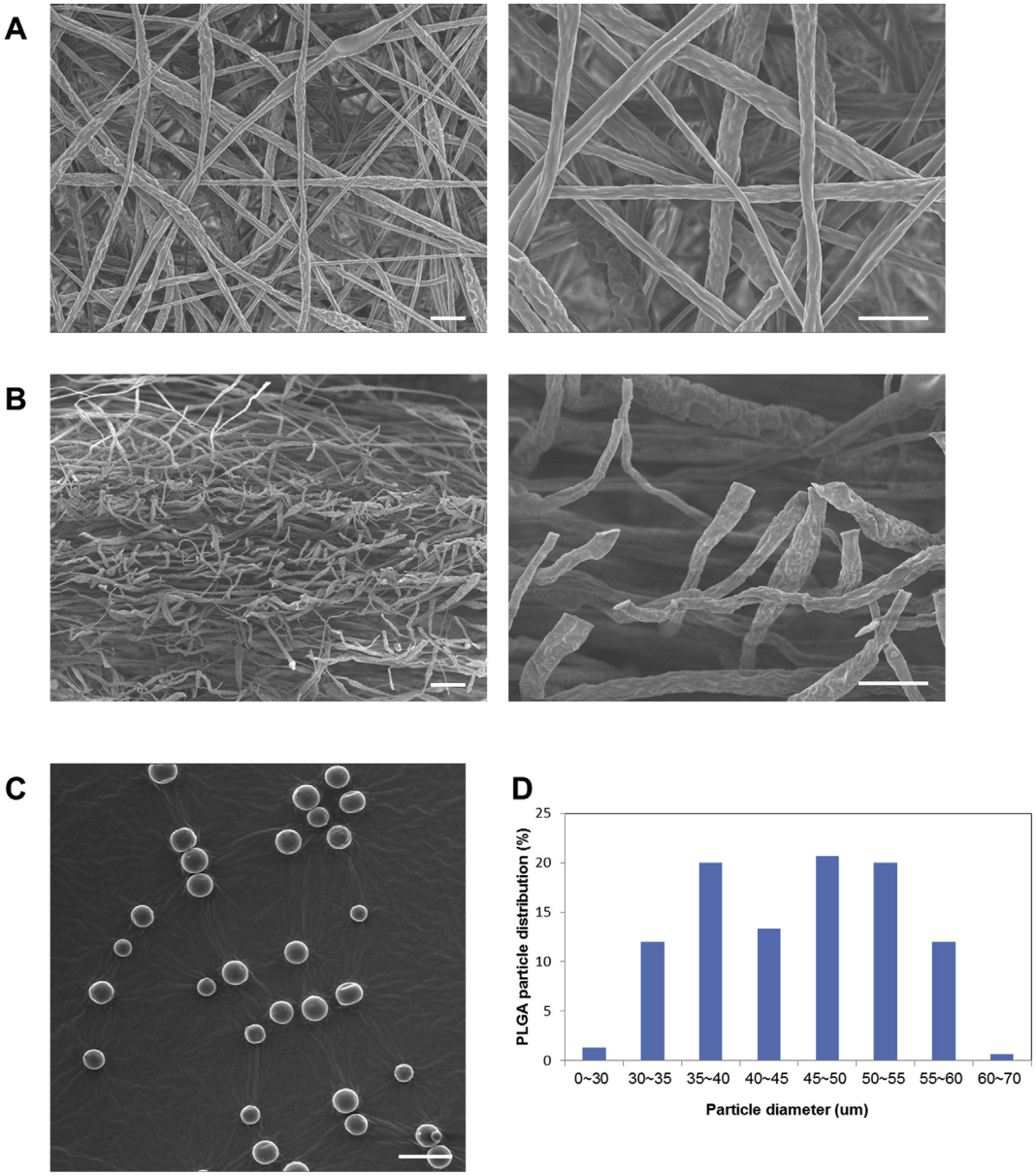

Fig. 3. Morphology of PLGA scaffold fabricated at low temperature and PLGA (50:50) particles were observed with SEM. (A) Surface of electrospun LT PLGA scaffold. Scale bar = 10 μm. (B) Cross section of electrospun LT PLGA scaffold. Scale bar = 10 μm. (C) SEM image of the PLGA (50:50) particles. Scale bar = 100 μm (D) Size distribution of the PLGA (50:50) particles. Number of measured particles was 150.

t-tests were used for unpaired data. A value of $p < 0.05$ is considered statistically significant.

3. Results and discussion

3.1. Effects of shear stress on hMSC migration

The modulation of hMSCs migration was first characterized by shear stress as a function of intensity. hMSCs were subjected to shear stress (8 dyne/cm^2, 16 dyne/cm^2) or kept as static control (0 dyne/cm^2). The migration speed and its directedness were calculated from the time-lapse microscopy (Fig. 2). Under static conditions (0 dyne/cm^2), hMSCs showed random migration without any preferential direction (Fig. 2A). The application of shear stress for 4 h, however, caused >80% (8 dyne/cm^2) or > 90% (16 dyne/cm^2) of cells to migrate in the flow direction (Fig. 2A). The effects of shear stress on the temporal change of cell migration speed (regardless of direction) are shown (Fig. 2B). After 4 h of shearing (16 dyne/cm^2), the migration speed significantly decreased by 50% above the preshear. Shear stress caused the value of directedness to increase significantly over that under static conditions (Fig. 2C). The directedness under 16 dyne/cm^2 was the highest value (0.715 ± 0.058) however the migration speed was decreased considerably. According to these results, we determined on 8 dyne/cm^2 of flow shear stress to apply to hMSCs. Mechanical forces are known to be important in a variety of cellular processes, actively participating in the regulation of cell growth, differentiation, gene expression and migration [6]. Cells are able to detect and respond to shear stress through mechanotransduction, a complex process that converts mechanical forces into biochemical signals and integrates these into a cellular response [7].

3.2. Low temperature electrospun PLGA (75:25) scaffold and PLGA (50:50) micro particles

A wide array of architectural configurations and geometries can be created using scaffold fabrication technologies such as rapid prototyping, melt extrusion, salt leaching, emulsion templating, phase separation, and electrospinning [19]. The electrospinning was chosen to fabricate the scaffold because electrospining is a process that can generate fiber mesh scaffolds with high porosities, large surface area-to-volume ratios, and variable fiber diameters [20,21]. These features, along with the versatility and simplicity of the system, make electrospinning an attractive tool for the production of scaffolds. The SEM images of low temperature electrospun PLGA (75:25) scaffold were shown in Fig. 3. The diameter of PLGA fibers was (1.55 ± 0.72) μm (Fig. 3A) and the thickness of the scaffold was (0.98 ± 0.14) mm. The thickness of the scaffold was measured using vernier-calipers. The edge of the low temperature scaffold could not be outlined because of its thickness (Fig. 3B).

The influence of process parameters on the fiber diameter and the inter-fiber spacing has therefore been investigated in detail and today allows adjusting the porosity or net density in flat structures [22–26]. The use of a low-temperature fiber collection device in air with controlled humidity allowed the simultaneous deposition of polymer fibers and ice particles from condensing humidity. The ice particles were intimately embedded within the polymer fibers and

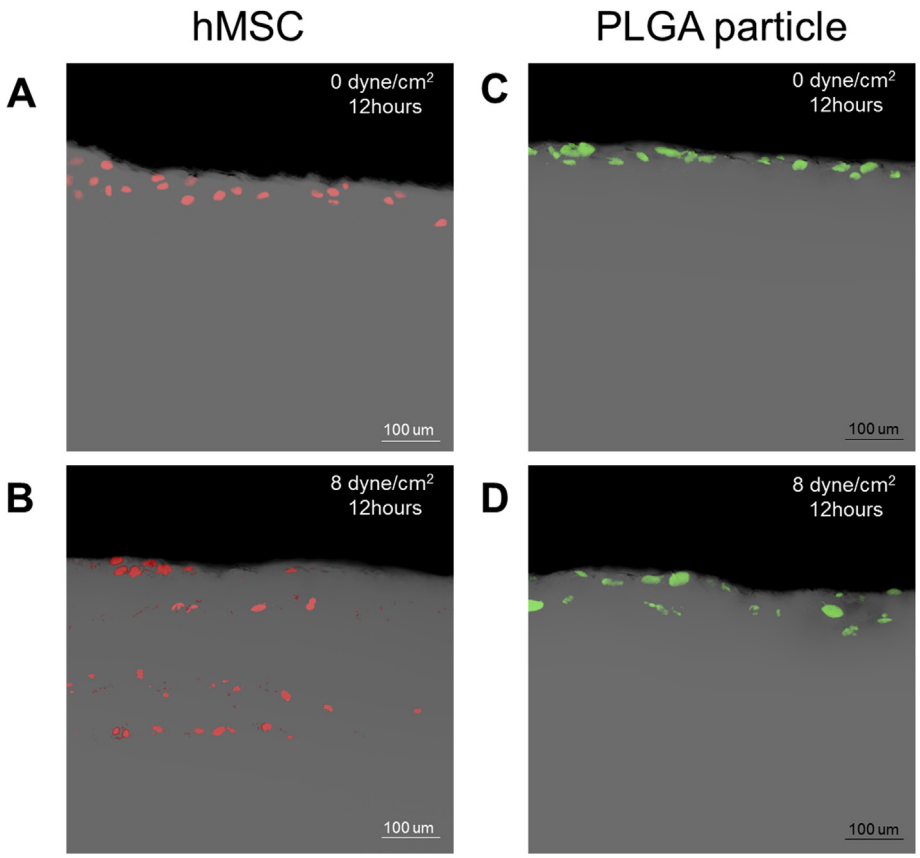

Fig. 4. The infiltration of hMSCs and PLGA particles into electrospun LT PLGA (75:25) scaffold under flow shear stress condition (0, 8 dyne/cm^2). Cross-sectional area of fluorescent image for cell distribution throughout the scaffold under (A) 0 dyne/cm^2 and (B) 8 dyne/cm^2 for 12 h. Cross-sectional area of fluorescent image for the PLGA (50:50) particle distribution throughout the scaffold under (C) 0 dyne/cm^2 and (D) 8 dyne/cm^2 for 12 h.

served as a pore template thus defining the scaffold porosity after drying of the collected fiber assemblies. This simple and well accessible use of ice crystals as void templates gives access to the preparation of biodegradable tissue engineering scaffolds with an up to four times higher porosity if compared to conventional fiber electrospinning [27].

The PLGA (50:50) particles were prepared to prove that the cells infiltrated into the scaffold by mechanotaxis. The diameters of suspended hMSCs were measured to determine the appropriate size of PLGA (50:50) particles and were 37.99 ± 6.39 μm (data not shown). The SEM image of PLGA micro particles is shown in Fig. 3(C) and particle size distribution is in Fig. 3(B). The particle size distribution was measured using the Image J software program on the basis of the scale bar in SEM images.

3.3. *The effect of fluid shear stress on the infiltration of hMSC and PLGA (50:50) particles into PLGA (75:25) scaffold*

To visualize hMSCs distribution inside the scaffolds after shear stress-induced cell migration cell-seeded scaffolds were stained with PI after the fixation and analyzed by confocal microscopy. Fig. 4(A) shows the cell distribution in the PLGA scaffold without flow shear stress. The cells under the flow shear stress condition (8 dyne/cm^2) migrated deeper than static conditions. The deepest distance of the cells under 8 dyne/cm^2 was 220.02 μm (Fig. 4B). The distance of infiltrated cells from the top surface of the PLGA scaffold was measured by using the Image J software program on the basis of the scale bar. These results suggest that flow shear stress enhances the infiltration of hMSCs into PLGA scaffold, however the reason that infiltration of hMSCs enhanced by flow shear stress still needs to be figured out either cells were pushed by mechanical force of flow shear stress or migrated into the scaffold actively by mechanotaxis.

The fluorescence images of PLGA (50:50) particle distribution in PLGA (75:25) scaffolds under static and fluid shear stress (8 dyne/cm^2) are shown (Fig. 4C and D). It is obvious that there is no significant differences of particle infiltration into scaffolds between static condition and fluid shear stress applied condition. These results support that hMSCs were not just pushed to the inside of scaffolds by physical force of fluid shear stress. Identifying the actual mechanism for mechanotaxis of hMSCs would constitute a major step towards verifying this hypothesis.

In summary, this study showed that the fluid shear stress enhanced the infiltration of hMSCs into PLGA scaffold. The cells moved along the direction of flow and they were also infiltrated into the PLGA scaffold by the fluid shear stress. However, the infiltration of PLGA micro particles into PLGA scaffolds was not affected by the fluid shear stress. These results suggest that the cells were infiltrated into the PLGA scaffold by responding to the fluid shear stress through the mechanotransduction. The enhancement of hMSCs infiltration into PLGA scaffold through fluid shear stress could be an important technique for promoting the cell infiltration into scaffolds for tissue engineering.

Acknowledgments

This research was supported by a grant of the Korea Healthcare technology R&D Project, Ministry for Health & Welfare, Republic of Korea (A 120878).

Conflict of interest

The authors have declared no conflict of interest.

Transparency document

Transparency document related to this article can be found online at http://dx.doi.org/10.1016/j.bbrc.2015.05.048.

References

[1] R. Langer, J.P. Vacanti, Tissue engineering, Science 260 (1993) 920–926.
[2] A.S. Mistry, A.G. Mikos, Tissue engineering strategies for bone regeneration, Adv. Biochem. Eng. Biotechnol. 94 (2005) 1–22.
[3] S. Xinfeng, S. Balaji, P. Quynh, L. Feng, A.G. Mikos, Fabrication of porous ultrashort single-walled carbon nanotube nanocomposite scaffolds for bone tissue engineering, Biomaterials 28 (2007) 4078–4090.
[4] S.P. Bruder, D.J. Fink, A.I. Caplan, Mesenchymal stem cells in bone development, bone repair and skeletal regeneration therapy, J. Cell. Biochem. 56 (1994) 283–294.
[5] D.J. Prockop, Marrow stromal cells as stem cells for nonhematopoietic tissues, Science 276 (1997) 71–74.
[6] A. Katsumi, W. Orr, E. Tzima, M.A. Schwartz, Integrins in mechanotransduction, J. Biol. Chem. 279 (2004) 12001–12004.
[7] H. Huang, R.D. Kamm, R.T. Lee, Cell mechanics and mechanotransduction: pathways, probes, and physiology, J. Physiol. Cell. Physiol. 287 (2004) C1–C11.
[8] L. Song, B. Peter, W. Yingxiao, H. Yingli, H. Shunichi, The role of the dynamics of focal adhesion kinase in the mechanotaxis of endothelial cells,, PNAS 99 (2009) 3546–3551.
[9] M.L. Tu, H.Q. Wang, X.D. Sun, L.J. Chen, Z.J. Ke, Pim-1 is upregulated by shear stress and is involved in shear stressinduced proliferation of rat mesenchymal stem cells, Life Sci. 88 (2011) 233–238.
[10] G. Yourek, S.M. McCormick, J.J. Mao, G.C. Reilly, Shear stress induces osteogenic differentiation of human mesenchymal stem cells, Regen. Med. 5 (2010) 713–724.
[11] Y. Huang, X. Jia, K. Bai, X. Gong, Y. Fan, Effect of fluid shear stress on cardiomyogenic differentiation of rat bone marrow mesenchymal stem cells, Arch. Med. Res. 41 (2010) 497–505.
[12] M.F. Pittenger, A.M. Mackay, S.C. Beck, R.K. Jaiswal, D.R. Marshak, Multilineage potential of adult human mesenchymal stem cells, Science 284 (1999) 143–147.
[13] I. Bab, C.R. Howlett, B.A. Ashton, M.E. Owen, Ultrastructure of bone and cartilage formed in vivo in diffusion chambers, Clin. Orthop. Relat. Res. 187 (1984) 243–254.
[14] A.J. Friedenstein, R.K. Chailakhyan, U.V. Gerasimov, Bone marrow osteogenic stem cells: in vitro cultivation and transplantation in diffusion chambers, Cell. Tissue Kinet. 20 (1987) 263–272.
[15] H.J. Mardon, J. Bee, K. Mark, M.E. Owen, Development of osteogenic tissue in diffusion chambers from early precursor cells in bone marrow of adult rats, Cell. Tissue Res. 250 (1987) 157–165.
[16] A.I. Caplan, Mesenchymal stem cells, Orthop. Res. 9 (1991) 641–650.
[17] M.A. Koo, J.K. Kang, M.H. Lee, H.J. Seo, B.J. Kwon, K.E. You, M.S. Kim, D.H. Kim, J.C. Park, Stimulated migration and penetration of vascular endothelial cells into poly (l-lactic acid) scaffold under flow conditions, Biomaterials Res. 18 (2014) 48–54.
[18] J. Liu, S.M. Zhang, P.P. Chen, L. Cheng, C.M. Ke, Controlled release of insulin from PLGA nanoparticles embedded within PVA hydrogels, J. Mater. Sci. Mater. Med. 18 (2007) 2205–2210.
[19] P.P. Quynh, S. Upma, A.G. Mikos, Electrospun Poly(E-caprolactone) microfiber and multilayer nanofiber/microfiber scaffolds: characterization of scaffolds and measurement of cellular infiltration, Biomacromolecules 7 (2006) 2796–2805.
[20] G.E. Wnek, M.E. Carr, D.G. Simpson, G.L. Bowlin, Electrospinning of nanofiber fibrinogen structures, Nano Lett. 3 (2003) 213–216.
[21] T. Subbiah, G.S. Bhat, R.W. Tock, S. Pararneswaran, S.S. Ramkumar, Electrospinning of nanofibers, J. Appl. Polym. Sci. 96 (2005) 557–569.
[22] D.H. Reneker, I. Chun, Nanometre diameter fibres of polymer, produced by electrospinning, Nanotechnology 7 (1996) 216–223.
[23] H. Fong, I. Chun, D.H. Reneker, Beaded nanofibers formed during electrospinning, Polymer 40 (1999) 4585–4592.
[24] C.Y. Xu, R. Inai, M. Kotaki, S. Ramakrishna, Aligned biodegradable nanofibrous structure: a potential scaffold for blood vessel engineering, Biomaterials 25 (2004) 877–886.
[25] L. Moroni, R. Licht, J.B. Boer, J.R. Wijn, C.A. Blitterswijk, Fiber diameter and texture of electrospun PEOT/PBT scaffolds influence human mesenchymal stem cell proliferation and morphology, and the release of incorporated compounds, Biomaterials 27 (2006) 4911–4922.
[26] M.M. Hohman, M. Shin, G. Rutledge, M.P. Brenner, Electrospinning and electrically forced jets. II. Applications, Phys. Fluids 13 (2001) 2221–2236.
[27] S. Marc, D.S. Oliver, N. Peter, J.S. Wendelin, 3D polymer meshes by low-temperature electrospinning: use of ice crystals as a removable void template, Polym. Eng. Sci. 47 (2007) 2020–2026.